5058 *Chem. Mater.* **2009,** *21,* 5058–5065
DOI:10.1021/cm9015047

CHEMISTRY OF MATERIALS
Article

Ferroelectric $BaTiO_3$ Nanowires by a Topochemical Solid-State Reaction

Maria Teresa Buscaglia,[†] Catalin Harnagea,[‡] Monica Dapiaggi,[§] Vincenzo Buscaglia,*[,†] Alain Pignolet,[‡] and Paolo Nanni[⊥,†]

[†]*Institute for Energetics and Interphases, National Research Council, Via De Marini 6, I-16149 Genoa, Italy,* [‡]*INRS-Energie, Matériaux et Telécommunications, University of Québec, 1650 boul. Lionel-Boulet, Varennes, Quebec, Canada J3X 1S2,* [§]*Department of Earth Sciences, University of Milano, Via Botticelli 23, I-20133 Milano, Italy, and* [⊥]*Department of Chemical and Process Engineering, University of Genoa, Piazzale Kennedy, I-16129 Genoa, Italy*

Received June 1, 2009. Revised Manuscript Received September 25, 2009

The possible existence of a new kind of ferroelectric order and the need to explore domain arrangement in ferroelectric nanostructures has stimulated an increasing activity on the growth of ferroelectric nanowires. In the present study, single crystal $BaTiO_3$ nanowires with tetragonal structure were obtained by an original solid-state process using layered titania nanowires coated with $BaCO_3$ nanocrystals as reactive templates. Formation of $BaTiO_3$ occurs at 700 °C by a topochemical reaction. Consequently, the initial morphology of the titania nanowires is retained in the final product. Piezoresponse force microscopy measurements show a strong piezoactivity and stripe domain patterns with domain width of 20−50 nm, predominant in-plane response and 90° domain walls. The proposed synthesis method is quite general and might be adapted to the fabrication different ferroelectric and nonferroelectric oxide nanowires.

1. Introduction

Ferroelectrics are one of the most intensively investigated class of materials because of their application in several kind of electronic devices including multilayer ceramic capacitors, ferroelectric nonvolatile memories (FeRAMs), piezoelectric transducers and actuators, pyroelectric sensors, and PTCR heating elements.[1−3] In particular the fabrication of one-dimensional (1D) ferroelectric nanostructures such as nanowires (NWs) and nanotubes (NTs) has received increasing attention in the recent years for two important reasons. First, the study of these systems can provide useful information for the fabrication of next generation, fully three-dimensional FeRAM structures with the required bit density.[3] In particular formation and arrangement of domains in ferroelectric nanostructure is not yet well established. Second, detailed ab initio calculations have predicted a new kind of ferroelectric order (circular or toroidal ordering of dipoles) in nanorods and nanodisks.[4] This could open a new avenue for the use of ferroelectric nanostructures in data storage. Fabrication of 1D ferroelectric structures is usually carried out by two main general methods: template-mediated approaches and direct growth from a liquid phase. $Pb(Zr,Ti)O_3$ (PZT) and $BaTiO_3$ NWs and NTs were prepared using suitable templates, such as silicon, alumina, and polycarbonate membranes, with ordered cylindrical pores which are infiltrated with a suitable liquid precursor.[3,5] Recently, NTs have been obtained by coating ZnO nanorods or Si nanowires with PZT using magnetron sputtering or pulsed laser deposition followed by chemical etching.[6] Direct growth of ferroelectric 1D nanostructures by chemical or solution methods is not trivial and not many reports have been published.[7] $BaTiO_3$ NWs with length reaching up >10 μm and diameter <100 nm were initially obtained by solvothermal synthesis using organic

*Corresponding author. Phone: +39-010-6475708; Fax: +39-010-6475700. E-mail: v.buscaglia@ge.ieni.cnr.it.

(1) (a) Damjanovic, D. *Rep. Prog. Phys.* **1998**, *61*, 1267. (b) Setter, N.; Damjanovic, D.; Eng, L.; Fox, G.; Gevorgian, S.; Hong, S.; Kingon, A.; Kohlstedt, H.; Park, N. Y.; Stephenson, G. B.; Stolitchnov, I.; Taganstev, A. K.; Taylor, D. V.; Yamada, T.; Streiffer, S. *J. Appl. Phys.* **2006**, *100*, 051606.
(2) Shaw, T. M.; Trolier-McKinstry, S.; McIntyre, P. C. *Annu. Rev. Mater. Sci.* **2000**, *30*, 263.
(3) Scott, J. F.; Morrison, F. D.; Miyake, M.; Zubko, P.; Lou, X.; Kugler, V. M.; Rios, S.; Zhang, M.; Tatsuta, T.; Tsuji, O.; Leedham, T. J. *J. Am. Ceram. Soc.* **2005**, *88*, 1691.
(4) (a) Naumov, I. I.; Bellaiche, L.; Fu, H. *Nature* **2004**, *432*, 737. (b) Fu, H; Bellaiche, L. *Phys. Rev. Lett.* **2003**, *91*, 257601. (c) Scott, J. F. *Nat. Mater.* **2005**, *4*, 13.
(5) (a) Limmer, S. J.; Seraji, S.; Wu, Y.; Chou, T. P.; Nguyen, C.; Cao, G *Adv. Func. Mater.* **2002**, *12*, 59. (b) Hernandez, B,A.; Chang, K. S.; Fisher, E. R.; Dorhout, P. K. *Chem. Mater.* **2002**, *14*, 480. (c) Luo, Y.; Szafraniak, I.; Zakharov, N. D.; Nagarajan, V.; Steinhart, M.; Wehrspohn, R. B.; Wendorff, J. H.; Ramesh, R.; Alexe, M. *Appl. Phys. Lett.* **2003**, *83*, 440. (d) Hirano, S.; Shimada, S.; Kuwabara, M. *Appl. Phys. A: Mater. Sci. Process.* **2005**, *80*, 783. (e) Kim, J.; Yang, S. A.; Choi, Y. C.; Han, J. K.; Jeong, K. O.; Yun, Y. J.; Kim, D. J.; Yang, S. M.; Yoon, D.; Cheong, H.; Chang, K.-S.; Noh, T. W.; Bu, S. D. *Nano Lett.* **2008**, *8*, 1813.
(6) Alexe, M.; Hesse, D.; Schmidt, V.; Senz, S.; Fan, H. J.; Zacharias, M.; Gösele, U. *Appl. Phys. Lett.* **2006**, *89*, 172907.
(7) (a) Cho, S.-B.; Oledzka, M.; Riman, R. E. *J. Cryst. Growth.* **2001**, *226*, 313. (b) Xu, G.; Ren, Z. H.; Du, P. Y.; Weng, W. J.; Shen, G.; Han, G. R. *Adv. Mater.* **2005**, *17*, 907. (c) Liu, J.-F.; Li, X.-L.; Li, Y.-D. *J. Nanosci. Nanotechnol.* **2002**, *2*, 617. (d) Suyal, G.; Colla, E.; Gysel, R.; Cantoni, M.; Setter, N. *Nano Lett.* **2004**, *4*, 1339. (e) Wang, J.; Sandu, C. S.; Colla, E.; Wang, Y.; Ma, W.; Gysel, R.; Trodahl, H. J.; Setter, N. *Appl. Phys. Lett.* **2007**, *90*, 133107.

 Published on Web 10/16/2009

solvents and metal alkoxides.[8] Single-crystal $BaTiO_3$ NWs were also grown in hydrothermal conditions at 170 °C using a ethanol−water mixture [9] as well as at high temperature (820 °C) from NaCl melts.[10] Transformation of layered alkaline titanates in barium titanate NTs/NWs by a topotactic reaction with barium hydroxide in hydrothermal conditions was also proposed, although with controversial results. Elongated platelets[11] and nanorods[12] were obtained from potassium titanate ($K_2Ti_4O_9$) precursors, while the use of sodium titanate often gave dendritic nanostructures.[13] Ferroelectric NWs can be also obtained by direct patterning of single crystal substrates, for example by focused ion beam etching.[14]

The possibility to obtain 1D nanostructures by solid-state reaction is largely unexplored.[15] The preparation of high-quality monocrystalline $ZnAl_2O_4$ nanotubes by solid-state reaction of ZnO nanowires coated with Al_2O_3 has been recently reported.[16] $MgAl_2O_4$ nanotubes and Zn_2TiO_4 nanowires were prepared by a similar route.[17] In this study we report a new method for the fabrication of ferroelectric $BaTiO_3$ nanowires based on the simple solid-state reaction between titania nanorods and a barium carbonate coating at moderate temperature.

2. Experimental Section

2.1. Synthesis of $BaTiO_3$ Nanowires. Fabrication of the $BaTiO_3$ NWs is carried using a three step procedure: (1) synthesis of layered hydrous titania nanowires (denoted in the following as LTNWs), (2) coating of the layered titania NWs with nanocrystalline $BaCO_3$, and (3) solid state reaction at 700 °C. The layered titania NWs as well as the final $BaTiO_3$ NWs were characterized by different methods.

Synthesis of Layered Titania Nanowires. In a typical synthesis, 3 g of ultrafine TiO_2 powder (VP TiO_2 P 90, Evonik Degussa GmbH, Hanau, Germany) are dispersed in 60 mL of a 10 M NaOH solution by vigorous stirring for 30 min. The resulting suspension is transferred in a 125 mL stainless steel PTFE-lined autoclave (model PA4748, Parr Instrument Company), heated in an oven at 4 °C min^{-1} up to 250 °C and kept at the reaction temperature for 5 h. The resulting precipitate, consisting of $Na_2Ti_4O_9$ NWs, is collected, washed several times alternating with distilled water and a 1 M HNO_3 solution, and finally aged overnight with 200 mL of a HNO_3 solution at pH 1 under stirring. The solid phase was always separated by high-speed centrifugation thus preventing a significant loss of very fine particles. The washing treatment determines the transformation of sodium titanate in layered hydrous titania by ion exchange while preserving the morphology of the starting NWs. The precipitate was finally washed twice with a 0.1 M HNO_3 solution by centrifugation, redispersed again in the HNO_3 solution using a ultrasonication horn. The resulting stable suspension was then freeze-dried resulting in a white and fluffy powder.

Coating of Titania Nanowires with $BaCO_3$. In a typical synthesis, 0.52 g of a very fine $BaCO_3$ powder (specific surface area: 28 m^2 g^{-1}, Solvay Bario e Derivati, Massa, Italy) were dispersed in 250 mL of a dilute NH_4OH solution at pH 8 by prolonged ultrasonication. A suspension of 0.24 g of LTNWs was prepared using the same procedure and heated at 90 °C. To obtain the correct stoichiometry Ba/Ti = 1 the weight loss of both the LTNW (after 6 h calcination at 800 °C) and $BaCO_3$ (after 6 h calcination at 600 °C) was taken into account. By calcination the LTNWS transform in anhydrous TiO_2 (see Results) while the nanocrystalline $BaCO_3$ loses adsorbed water and organic additives. The $BaCO_3$ suspension was slowly added to the TiO_2 suspension while stirring. After complete addition, the suspension was kept at 90 °C for 30 min. Finally, the solid phase was separated by centrifugation and then freeze-dried.

Solid-State Reaction. The TiO_2−$BaCO_3$ powder was put in a platinum crucible and calcined for 6 h at 700 °C in air.

2.2. Characterization. Phase composition was determined by conventional X-ray diffraction (XRD, Philips PW1710). Synchrotron powder diffraction data of the $BaTiO_3$ NWs were collected in transmission mode at beamline ID31 of the European Synchrotron Radiation Facility (ESRF, Grenoble, France), by utilizing high-energy X-rays (wavelength ≈ 0.4 Å) at room temperature. The scanned angular range extends down to $d = 0.59$ Å and includes all $BaTiO_3$ reflections from (100) to (631). Thus, for the tetragonal structure, 129 independent reflections are available. Structure refinement was performed by the Rieveld method using the GSAS-EXPGUI software.[18] Morphology was observed by scanning (SEM, LEO 1450 VP) and transmission electron microscopy (TEM, FEI Tecnai F20 and JEOL J2010). The TEM was equipped with an energy dispersive electron microprobe (EDS, Oxford Instruments) for measurement of elemental composition. Differential scanning calorimetry (DSC, Mettler Toledo) measurements were performed in the range 300−425K with a heating/cooling rate of 10 K/min.

2.3. Piezoresponse Force Microscopy. The ferroelectric properties of individual $BaTiO_3$ NWs were investigated at local scale using piezoresponse force microscopy (PFM). First, the samples were prepared as follows: a small amount of the NW-powder was dispersed in acetone by ultrasonication, and few droplets of the resulting suspension were deposited on a platinum-coated alumina substrate and dried. Because the instrument is operated in contact mode, the force between the tip and sample is strong enough to move the NWs while scanning across the surface. To

(8) (a) Urban, J. J.; Yun, W. S.; Gu, Q.; Park, H. *J. Am. Chem. Soc.* **2002**, *124*, 1186. (b) Yun, W,S.; Urban, J. J.; Gu, Q.; Park, H. *Nano Lett.* **2002**, *2*, 447. (c) Urban, J. J.; Spanier, J. E.; Lian, O. Y.; Yun, W,S.; Park, H. *Adv. Mater.* **2003**, *15*, 423.
(9) (a) Joshi, U. A.; Lee, S. *Small* **2005**, *1*, 1172. (b) Joshi, U. A.; Yoon, S.; Baik, S.; Lee, S. *J. Phys. Chem. B* **2006**, *110*, 12249.
(10) (a) Mao, Y.; Banerjee, S.; Wong, S. S. *J. Am. Chem. Soc.* **2003**, *125*, 15718. (b) Wang, Z.; Hu, J.; Yu, M.-F. *Appl. Phys. Lett.* **2006**, *89*, 263119.
(11) Feng, Q.; Hirasawa, M.; Yanagisawa, K. *Chem. Mater.* **2001**, *13*, 290.
(12) Kang, S.-O.; Park, B. H.; Kim, Y.-I. *Cryst. Growth. Des.* **2008**, *8*, 3180.
(13) (a) Maxim, F.; Ferreira, P.; Vilarinho, P.M.; Reaney, I. *Cryst. Growth. Des.* **2008**, *8*, 3309. (b) Bao, N.; Shen, L.; Srinivasan, G.; Yanagisawa, K.; Gupta, A. *J. Phys. Chem. C* **2008**, *112*, 8634.
(14) (a) Schilling, A.; Bowman, R. M.; Catalan, G.; Scott, J. F.; Gregg, J. M. *Nano Lett.* **2007**, *7*, 3787. (b) Schilling, A.; Bowman, R. M.; Gregg, J. M.; Catalan, G.; Scott, J. F. *Appl. Phys. Lett.* **2006**, *89*, 212902.
(15) (a) Fan, H. J.; Gösele, U.; Zacharias, M. *Small* **2008**, *3*, 1660. (b) Bae, C.; Yoo, H.; Kim, S.; Lee, K.; Kim, J.; Sung, M. M.; Shin, H. *Chem. Mater.* **2008**, *20*, 756.
(16) Fan, H. J.; Knez, M.; Scholz, R.; Nielsch, K.; Pippel, E.; Hesse, D.; Zacharias, M.; Gösele, U. *Nat. Mater.* **2006**, *5*, 627.
(17) (a) Fan, H. J.; Knez, M.; Scholz, R.; Nielsch, K.; Pippel, E.; Hesse, D.; Gösele, U.; Zacharias, M. *Nanotechnology* **2006**, *17*, 5157. (b) Yang, Yi; Sun, Xiao Wei; Tay, Beng Kang; Wang, Jian Xiong; Dong, Zhi Li; Fan, Hai Ming *Adv. Mater.* **2007**, *19*, 1839. (c) Yang, Y.; Scholz, R.; Fan, H. J.; Hesse, D.; Gösele, U.; Zacharias, M. *ACS Nano* **2009**, *3*, 555.
(18) (a) Larson, C.; Von Dreele, R. B., *General Structure Analysis System* (*GSAS*), Los Alamos National Laboratory, Los Alamos, NM, 1994, pp 86−748;(b) Toby, B. H. *J. Appl. Crystallogr.* **2001**, *34*, 210.

avoid the uncontrolled displacement of the small 1D structures during the measurement, the substrate was then thermally treated for 2 h at 500 °C to induce adhesion of the NWs on the metal surface. The PFM technique, based on the converse piezoelectric effect, detects small local sample surface oscillations induced by an ac electric field applied between the conductive tip and a sample back electrode. Here we used the experimental setup described earlier:[19] an Enviroscope atomic force microscope (Veeco) equipped with CSC37 cantilevers and tips coated with Ti/Pt from Mikromasch. We used relatively soft cantilevers ($k \sim 0.2$ N/m) in order to achieve a low contact force of 10 nN. For imaging, we used a very low excitation amplitude of 0.1 V at frequencies as high as possible for in-plane detection (35 kHz). The resulting piezoelectric deformations transmitted to the cantilever and both out-of-plane and in-plane components are detected from the global deflection signal using two Lock-in amplifiers (Signal Recovery, model 7265). For hysteresis measurements we used a dc source (Keithley 2400 Sourcemeter) in series with the AC driving voltage and swept the dc voltage between −1 and 1 V. It was impossible to keep the tip fixed on top of the NW using soft cantilevers, the power supply showed shortcircuit conditions, suggesting that the tip has slid on the metal electrode. Therefore, for hysteresis loop measurements we used somewhat stiffer cantilevers (CSC36 with $k \sim 1$ N/m) and therefore a higher contact force ~ 200 nN. For positioning the tip on top of the NW, we first used the noncontact mode of operation, and switched to contact mode only during the hysteresis measurement.

3. Results

3.1. Structure and Morphology of Layered Titania NWs. As shown by Pradhan et al.,[20] determination of crystal structure and composition of layered titania nanostructures is not a trivial problem. The diffraction pattern of the LTNWs obtained by acidic washing is shown in Figure 1a. It is similar to the patterns reported for $H_2Ti_3O_7$, $H_2Ti_2O_5 \cdot H_2O$ and titanates with lepidocrocite structure.[21] The strongest peak at about $2\theta = 12.6°$ should corresponds to the distance (0.82 nm in this case) between two adjacent layers of TiO_6 octahedra. The weight loss at 600 °C of the freeze-dried powder matches closely with that expected for the compound $H_2Ti_2O_5 \cdot H_2O$. The diffraction pattern of the LTNWs after calcination at 700 °C (Figure 1b) corresponds to single phase anatase TiO_2. This indicates that sodium has been efficiently removed from the sodium titanate NWs by the acidic washing. The morphology of the sodium-free LTNWs is shown in Figure 2. The fiber-like crystals have a width of 30−250 nm and a length from a few micrometers to >10 μm. The high-resolution image of Figure 2b indicates the single crystal nature of the LTNWs. The lattice fringes are parallel to the elongation direction of the crystals with a separation of about 0.7 nm. This separation corresponds to the interlayer distance observed by HRTEM in $H_2Ti_3O_7$ and $H_2Ti_2O_5 \cdot H_2O$ nanotubes.[20,21]

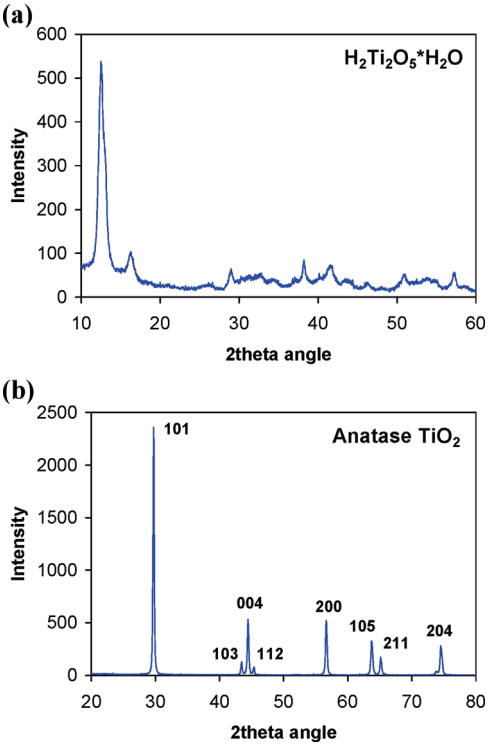

Figure 1. XRD patterns (Co Kα radiation) of (a) $H_2Ti_2O_5 \cdot H_2O$ nanowires. (b) Layered hydrous titania nanowires after calcination at 700 °C.

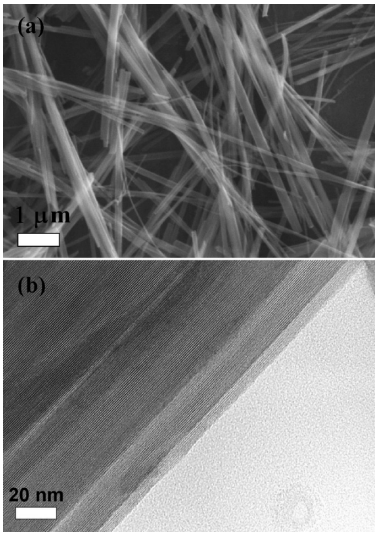

Figure 2. Morphology of the layered hydrous titania nanowires. (a) SEM (b) HR-TEM.

3.2. Structure and Morphology of $BaTiO_3$ NWs. Representative SEM and TEM images of the barium titanate NWs are reported in Figure 3. The NWs have a width between 50 and 300 nm and a length of 2−30 μm. According to AFM measurements, the NWs possess a rectangular section and they lie on the substrate with their shortest dimension (i.e., the thickness) perpendicular to the substrate surface. NWs with a length of a few micrometers and a width of 100−200 nm have a thickness of 50−70 nm. In the case of NWs with regular morphology, ED patterns taken at different distances along the same NW show the same diffraction pattern with sharp diffrac-

(19) Harnagea, C.; Cojocaru, C. V.; Nechache, R.; Gautreau, O.; Rosei, F.; Pignolet, A. *Int. J. Nanotechnol.* **2008**, *5*, 930.
(20) Pradhan, S. K.; Mao, Y.; Wong, S. S.; Chupas, P.; Petkov, V. *Chem. Mater.* **2007**, *19*, 6180.
(21) Tsai, C.-C.; Teng, H. *Chem. Mater.* **2006**, *18*, 367.

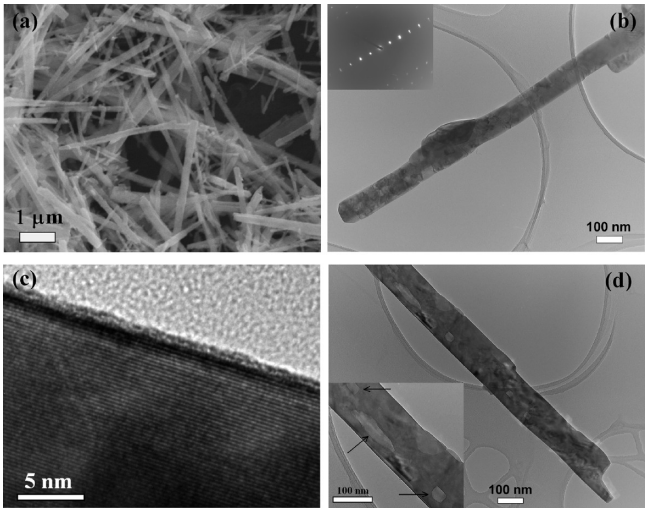

Figure 3. Morphology of $BaTiO_3$ nanowires. (a) SEM (b-d) TEM and HR-TEM. The inset of part (b) shows the ED pattern of the nanowire. The inset of part (d) evidence some defects.

tion spots (an example is given in the inset of Figure 3b), indicating that the NWs are single crystals. The most frequently observed lattice fringes are oriented parallel to the major axis of the nanorods and have a separation of about 0.27 nm (Figure 3c). This distance matches well with the separation of the (110), (101), and (011) planes of $BaTiO_3$ (0.28 nm, ICDD PDF 5-0626). Consequently, the elongation direction of the nanowires is parallel to one of the above lattice planes. Further details about nanowire morphology are given in Ferroelectric Properties of $BaTiO_3$ NWs section. NWs with less regular morphology are composed of two or more segments. Protuberances are often observed on the NW surface, as that shown in Figure 3b. PFM has revealed no piezoactivity in these surface structures, meaning that they are not composed of $BaTiO_3$. EDS analysis indicated that the majority of the protuberances are enriched in Ba with respect to the NWs composition. Considering that (i) XRD clearly showed the presence of a small amount of $BaCO_3$ (see below) and (ii) isolated particles of $BaCO_3$ were not observed, we conclude that the protuberances on the NW surface are most likely composed of $BaCO_3$. Dislocations, grain boundaries, and internal pores (see Figure 3d) were also detected inside the NWs.

The high-energy (wavelength ≈ 0.4 Å) XRD pattern of the NWs is reported in Figure 4. The main reaction product is $BaTiO_3$ beside minor amounts of $BaCO_3$ witherite (6.7 wt %) and $BaTi_4O_9$ (1.8 wt.%). The conventional XRD pattern (not shown) of the same material annealed for 2 h at 1350 °C (at this temperature complete equilibrium is attained) does not reveal any secondary phase. This indicates that Ba/Ti ratio is very close to one and, consequently, the secondary phases are mainly related to incomplete reaction rather than to deviation from the correct stoichiometry. Barium titanate possesses a perovskite structure. Above the Curie temperature (125 °C), the structure is cubic and paraelectric. Three different ferroelectric polymorphs appear at lower temperatures as a result of

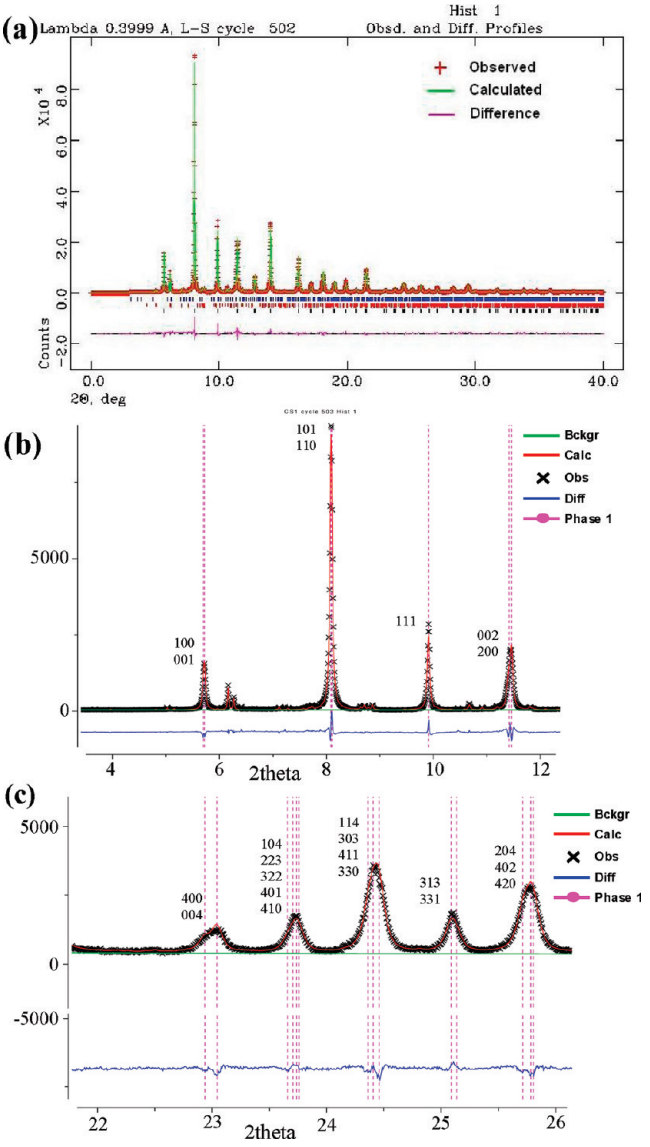

Figure 4. Rietveld fit of the synchrotron high-energy X-ray diffraction data (wavelength ≈ 0.4 Å). (a) Full pattern. Blue ticks: tetragonal $BaTiO_3$; red ticks: orthorhombic $BaCO_3$; black ticks: $BaTi_4O_9$. (b) Region 4−12°2θ. (c) Region 22−26°2θ.

small deformations of the cubic cell.[22] The structure is tetragonal between 125 and 0 °C, orthorhombic between 0 and −90 °C and rhombohedral below −90 °C. However, a shift of the transition temperatures has been reported in nanoparticles and nanoceramics, with the orthorhombic/tetragonal transition moving to higher temperature and the tetragonal to cubic transition to lower temperature with decreasing particle size.[23,24] The

(22) Kwei, G. H.; Lawson, A. C.; Billinge, S. J. L.; Cheong, S.-W. *J. Phys. Chem.* **1993**, *97*, 2368.
(23) (a) Frey, M. H.; Payne, D. A. *Phys. Rev. B* **1996**, *54*, 3158. (b) Polotai, A. V.; Ragulya, A. V.; Randall, C. *Ferroelectrics* **2003**, *288*, 93.
(24) (a) Uchino, K.; Sadanaga, E.; Hirose, T. *J. Am. Ceram. Soc.* **1989**, *72*, 1555. (b) Li, X.; Shih, W.-H. *J. Am. Ceram. Soc.* **1997**, *80*, 2844. (c) Ishikawa, K.; Uemori, T. *Phys. Rev. B* **1999**, *60*, 11841. (d) Tsunekawa, S.; Ito, S.; Mori, T.; Ishikawa, K.; Li, Z.-Q.; Kawazoe, Y. *Phys. Rev. B* **2000**, *62*, 3065. (e) Zhao, Z.; Buscaglia, V.; Viviani, M.; Buscaglia, M. T.; Mitoseriu, L.; Testino, A.; Nygren, M.; Johnsson, M.; Nanni, P. *Phys. Rev. B* **2004**, *70*, 024107. (f) Hoshina, T.; Kakemoto, H.; Tsurumi, T.; Wada, S.; Yashima, M. *J. Appl. Phys.* **2006**, *99*, 054311.

Table 1. Results of Rietveld Refinement of the Synchrotron Diffraction Data ($\lambda \approx 0.4$ Å) Collected from the $BaTiO_3$ Nanowires with the Orthorhombic *Amm2* Structure Model[a]

	this work	Kwei et al.,[22] 270 K
a (Å)	4.0011 (1)	3.9874
b (Å)	5.6785 (3)	5.6751
c (Å)	5.6880 (5)	5.6901
cell volume (Å^3)	129.23	128.76
Δz_{Ti}	0.0168 (29)	0.0169
Δz_{O1}	−0.0340 (7)	−0.0090
Δy_{O2}	0.0188 (5)	0.0060
Δz_{O2}	−0.0128 (6)	−0.0140
R_p	7.42%	
R_{wp}	10.27%	
X^2_{red}	12.32	

[a] Values in brackets represent the esd on the last decimal digit. Atomic positions: Ba (0,0,0), Ti(1/2,0,1/2 + Δz_{Ti}), O1(0,0,1/2 + Δz_{O1}), O2(1/2,1/4 + Δy_{O2}, 1/4 + Δz_{O2}).

Table 2. Results of Rietveld Refinement of the Synchrotron Diffraction Data ($\lambda \approx 0.4$ Å) Collected from the $BaTiO_3$ Nanowires with the Tetragonal *P4/mmm* Structure Model[a]

	this work	Kwei et al.,[22] 300 K
a (Å)	4.0049 (1)	3.99095
c (Å)	4.0230 (2)	4.0352
c/a	1.0045	1.0111
cell volume (Å^3)	64.526	64.271
Δz_{Ti}	0.0153 (3)	0.0224
Δz_{O1}	−0.0274 (7)	−0.0244
Δz_{O2}	−0.0112 (9)	−0.0105
R_p	7.38%	
R_{wp}	10.06%	
X^2_{red}	11.86	

[a] Values in brackets represent the esd on the last decimal digit. Atomic positions: Ba (0,0,0), Ti(1/2,1/2,1/2+Δz_{Ti}), O1(1/2,1/2,Δz_{O1}), O2(1/2,0,1/2+Δz_{O2}).

distortion of the unit cell is accompanied by a displacement of Ti and O ions from their highly symmetric positions. This gives rise to a net electrical dipole in the unit cell and the spontaneous polarization in the ferroelectric phases. In the high-temperature cubic phase no reflections are split. In the tetragonal phase, only the (*hhh*) reflections remain single peaks whereas the other reflections split into two or three components. Peak splitting is also observed for the orthorhombic and rhombohedral phases. In nanocrystalline $BaTiO_3$, peak splitting is usually not observed because of the small spontaneous strain and of the size broadening effect. Rather the peaks are broadened and slightly asymmetric, as shown in Figure 4 for the NWs of this study. Consequently, determination of the correct symmetry of nanostructured barium titanate is not trivial. Indeed, structure refinement with both the tetragonal and the orthorhombic structure produced a good match between calculated and experimental XRD patterns. The results of structure refinement (lattice parameters and atomic positions) are reported in Table 1 for the orthorhombic structure and Table 2 for the tetragonal structure. The fit provided by the *P4/mmm* tetragonal model is only marginally better (R_{wp}: 10.06%, R_p: 7.38%, χ^2_{red}: 11.86) than the one obtained with the orthorhombic *Amm2* structure (R_{wp}: 10.27%, R_p: 7.42%, χ^2_{red}: 12.32). However, the tetragonal structure is preferred for two reasons: (i) the asymmetry of some peaks (those originated by the splitting of the *h00* reflections for instance) is better described by the *P4/mmm* model, and (ii) the atomic displacements Δz_{O1} and Δy_{O2} obtained with the orthorhombic model (see Table 1) are much larger (four and three times, respectively) than the reference data reported in the literature [22] and this seems rather unrealistic. In contrast, the tetragonal model provides more realistic values of the Ti and O displacements (see Table 2). However, possible coexistence of both crystallographic modifications can not completely excluded.

Let us consider in more detail the refinement performed with the *P4/mmm* model structure (Table 2). The tetragonality, defined as the ratio c/a of the lattice parameters, is 1.0045, to be compared with the reference value of 1.011 obtained by neutron diffraction on coarse-grained ceramics.[22] A depressed tetragonality is a common feature of $BaTiO_3$ nanoparticles and nanoceramics [24,25] as well as of $BaTiO_3$ nanorods grown by solvothermal and hydrothermal methods.[8,9,12] The unit cell volume shows an expansion of about 0.5% in comparison to the reference value (see Table 2). Again, this is a common behavior of $BaTiO_3$ nanocrystals.[24,25] The displacements found for oxygen along the *c* direction, −0.027 Å for O_1 and −0.011 Å for O_2, are in fair agreement with previous determinations. In contrast, the off-center displacement Δz_{Ti} of Ti, 0.0153 Å, is substantially lower than the value of 0.0224 Å reported by Kwei et al.,[22] resulting in a smaller value of the spontaneous polarization and a reduced spontaneous strain (tetragonality).

3.3. Ferroelectric Properties of $BaTiO_3$ NWs. AFM measurements were possible only on relatively small NWs. Due to the poor adhesion on the surface, NWs longer than 3−4 μm and higher than 100 nm were moved away during scanning in contact by the lateral force exerted by the AFM tip. The NW shown in Figure 5 is 1.8 μm long, 150 nm wide (fwhm, full width at half-maximum) and protrudes 47 nm out of the surface. Analyzing the topographic data, we notice that the surface of the NWs is not flat, but exhibits a roughness of 1−3 nm. We associate this roughness to the formation of outgrows (arrow in Figure 5) of a secondary phase, probably $BaCO_3$, as suggested by EDS analysis and XRD.

PFM measurements (Figure 5) revealed that, while few NWs did not show a clear piezoelectric response, they exhibit, in general, a complex domain structure. Most frequently we observed stripe domain patterns with a characteristic width (fwhm) between 20 and 50 nm. Analyzing the contrast change between domains, we measure a domain wall width of 9 nm, a value which we associate with the ultimate resolution achievable in our experiment. Therefore we conclude that domains smaller that 20 nm are not resolved by our measurement. The ferroelectric nature of the NWs is proven by local piezoelectric hysteresis loops as shown in Figure 5c (not recorded from the

(25) Smith, M. B.; Page, K.; Siegrist, T.; Redmond, P. L.; Walter, E. C.; Seshadri, R.; Brus, L. E.; Steigerwald, M. L. *J. Am. Chem. Soc.* **2008**, *130*, 6955.

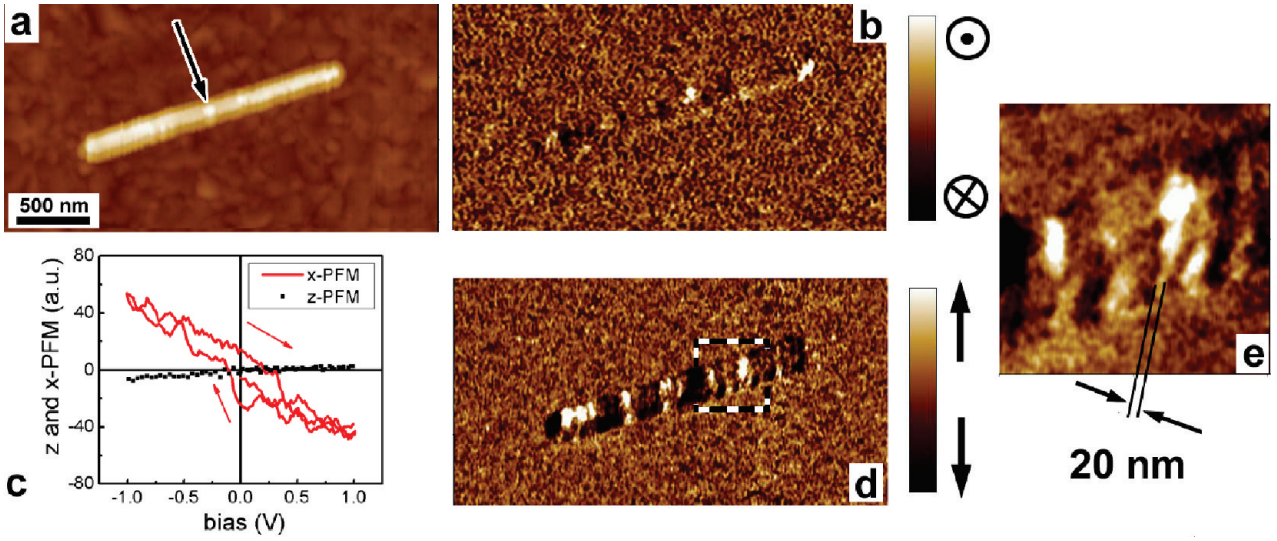

Figure 5. PFM experiment on a $BaTiO_3$ nanowire. (a) topography, (b) z-PFM, (c) x-PFM hysteresis loop, (d) x-PFM image, and (e) zoom of the region marked by a square in (d).

same NW). Analyzing the images, the NW exhibits a hysteretic in-plane response (Figure 5d), but not in the out-plane direction (Figure 5b). We therefore conclude that generally the polarization lies perpendicular to the shortest dimension of the NWs (i.e., the thickness) or, in other words, parallel to to the substrate. The observed domain structure, with domain walls approximately perpendicular to the elongation direction of the NWs and predominant in-plane polarization, is compatible with the existence of 90° domain walls in nanowires with major axis parallel the [−101] direction. The domain pattern can be inferred assuming that the surface scanned by PFM is parallel to the (010) planes. According to this morphology, the (101) planes lie parallel to the major axis of the NW, in agreement with the HRTEM results (Figure 2c), and perpendicular to the domain walls. In practice, this relatively simple picture of the domain structure is perturbed by the presence of some 180° domain walls and a few domains with out-of-plane polarization (Figure 5b and d).

DSC measurements showed no evidence of a latent heat, which is typical of a first order transition, in the range 300−425K. This indicates that the paraelectric to ferroelectric transition in $BaTiO_3$ NWs is of second order rather than of first order as observed in coarse particles and ceramics.

4. Discussion

Results from SEM, TEM, and AFM observations suggest that the $BaTiO_3$ nanowires directly originate from the titania NWs as a result of a topochemical solid-state reaction with $BaCO_3$. It is well assessed that growth of $BaTiO_3$ during the $BaCO_3$−TiO_2 reaction occurs by coupled diffusion of oxygen and barium ions through the perovskite layer.[26,27] Moreover, the perovskite layer was observed to grow with a well-defined orientation relationship with the TiO_2 substrate. Consequently, when the LTNWs are coated with $BaCO_3$, formation of barium titanate starts at the titania surface and the $BaTiO_3/TiO_2$ interface then gradually moves from the surface toward the center of the nanowire. Therefore, the process will end with formation of a dense single-crystal $BaTiO_3$ nanowire. Recent results on the growth of $BaTiO_3$ at 700 °C in thin-film diffusion couples obtained by evaporation of $BaCO_3$ on rutile single crystals support this interpretation.[28] A complementary situation is encountered when elongated $BaCO_3$ crystals are encapsulated with a titania shell:[29] the reaction leads to the formation of hollow $BaTiO_3$ particles. In this case the constrained geometry of the system does not allow for an efficient annihilation of the vacancies resulting from outward diffusion of Ba and O ions and enhances the formation of Kirkendall porosity at the $BaTiO_3/BaCO_3$ interface. Pore coarsening and coalescence by surface diffusion then determines the formation of a single central cavity. In contrast, during the reaction of $BaCO_3$-coated titania NWs, the formation of a rather dense reaction product (Figure 3) indicates that vacancies can be efficiently annihilated near the $BaTiO_3/BaCO_3$ interface. However, the internal pores observed in some of the NWs (see Figure 3) indicate that formation of Kirkendall porosity might occur to some extent. A further source of porosity and other defects, such as dislocations and internal boundaries, is represented by the elastic stresses. For a substrate with an infinite plane surface, the reaction layer can, in principle, collapse on the retreating reactant surface without stress generation if the reaction takes place uniformly over the

(26) Beauger, A.; Mutin, J. C.; Niepce, J. C. *J. Mater. Sci.* **1983**, *18*, 3041.
(27) Graff, A.; Senz, S.; Voltzke, D.; Abicht, H.-P.; Hesse, D. *J. Eur. Ceram. Soc.* **2005**, *25*, 2201.
(28) (a) Lotnyk, A.; Senz, S.; Hesse, D. *Solid State Ionics* **2006**, *177*, 429. (b) Lotnyk, A.; Senz, S.; Hesse, D. *Acta Mater.* **2007**, *55*, 2671.
(29) (a) Buscaglia, M. T.; Buscaglia, V.; Viviani, M.; Dondero, G.; Röhrig, S.; Rüdiger, A.; Nanni, P. *Nanotechnology* **2008**, *19*, 225602. (b) Buscaglia, M. T.; Buscaglia, V.; Alessio, R. *Chem. Mater.* **2007**, *19*, 711.

surface. For particles with finite dimensions, like the present nanowires, constraints are imposed on the system and this can produce cracks and voids at the interfaces or within the reaction layers. Deviations from the ideal behavior can arise also from a noncompletely uniform coating of the titania NWs that determines local variations of nucleation and reaction conditions. This is probably the reason for the non complete reaction observed at 700 °C. According to TEM and PFM observations (see Figure 3), residual barium carbonate forms the protuberances observed on the surface of the NWs. The phase $BaTi_4O_9$ originates form the locally incomplete reaction and, according to the reaction mechanism, it should be mainly located in the core of the $BaTiO_3$ NWs. An increase of the calcination temperature to 800 °C leads to nearly single phase $BaTiO_3$ but also to a strong aggregation of the NWs and the collapse of the finest structures with formation of aggregates of nanoparticles.

It is well-known that, when the particle/grain size is reduced below ≈100 nm, nanoparticles and nanoceramics of ferroelectric perovskites show a progressive lowering of spontaneous strain and Curie temperature.[24] In the case of $BaTiO_3$ NWs obtained by solvothermal synthesis, a significant decrease of T_C has been observed when the diameter is reduced below 20 nm.[30] In the present case, considering that the thickness of the smaller nanowires is on the order of 50−70 nm, the reduced tetragonality of the nanowires (1.0045, Table 2) in comparison to the reference value (1.011) is likely to be mainly the consequence of the existence of various extended defects inside the nanowires, including nanopores, interface boundaries, and dislocations. These defects and the related local elastic stresses can determine a significant relaxation of the constituting ions from the regular positions of the lattice resulting in substantial positional disorder.[25,31,32] In turn, positional disorder will lead to a partial loss of the long-range ferroelectric order and to a reduced average spontaneous strain and polarization. The negative impact of extended defects and their long-range strain field on the polarization of ferroelectric nanostructures has been shown both theoretically[33] and experimentally.[34] Recent results obtained by the analysis of high-energy X-ray diffraction data and pair distribution functions clearly indicate that disorder has a strong impact on the ferroelectric order and related properties of barium titanate nanoparticles and nanoceramics.[32] The presence of defects and disorder in the perovskite structure may be also the reason for the observed change of the order of the tetragonal/cubic phase transition, from first order to higher order. Nanowires with less defects and, consequently, improved ferroelectric properties, could be obtained by growing a BaO or $BaCO_3$ layer of uniform thickness by means of a gas phase deposition process, such as chemical vapor deposition or atomic layer deposition.

There are different orientations of the polarization compatible with the existence of ⟨110⟩ pseodocubic planes parallel to the major axis of the nanowires, as shown by HRTEM. For instance, if the nanowires were grown in the [001] direction, the (110) lattice planes, the polar *c*-axis and the polarization would be parallel to the elongation direction of the nanowire. However, the piezoresponse contrast (Figure 5) suggests that spontaneous polarization is not parallel to the NW longitudinal axis as it would be favored by the shape anisotropy. Recent results by Schilling et al.[14,35] on $BaTiO_3$ lamellae and nanocolumns with rectangular cross-section cut along the major crystallographic axes from bulk single crystalline $BaTiO_3$ using focused ion beam showed a similar trend: the equilibrium domain structure shows head−tail 90°-stripe domains. The width of the domains with polarization parallel to the wire axis (axial) is equal to the width of those with polarization perpendicular to it (nonaxial). Domains with nonaxial polarization form such that the polarization is perpendicular to the shortest lateral dimension of the column in order to minimize the depolarization energy. Simple theoretical models[14a] taking into account the surface energy density of domains U and the domain wall energy density γ point to the following relationship between the domain width w and the column width d at constant thickness: $w^2 = \gamma d/U$. The experimental value of the slope w^2/d approximately equals 10 nm.[35] Using this value for the slope and the width and thickness of the NW from Figure 5 we find that the equilibrium domain width for our geometry is predicted by the model to be ∼22 nm. Indeed, we find that the size of the smallest clearly defined domain is about 20 nm (Figure 5), confirming the prediction. The nearly absence of an out-of-plane PFM signal is again in agreement with the model, since the shortest dimension of the NW is its thickness, and therefore polarization lies parallel to the surface. We also observed domains with much larger sizes, in the 50−100 nm range, as well as few 180° domain walls and small domains with polarization perpendicular to substrate. These domain states in our NWs can be explained by the presence of defects, expected to significantly modify the total free energy of the NWs and thus affect the electrostatic energy governing the domain formation. Furthermore, the presence of defects has a strong influence on the nucleation and orientation of ferroelectric domains.

Despite the reduced tetragonality, the $BaTiO_3$ NWs are undoubtedly ferroelectric. It is important to emphasize here that the piezoelectric hysteresis loop shown in Figure 5c clearly demonstrates that the domains in our nanowires can be switched by an external electric field. The estimated effective coercive field is 39 kV/cm, about

(30) Spanier, J. E.; Kolpak, A. M.; Urban, J. J.; Grinberg, I.; Lian, O. Y.; Yun, W. S.; Rappe, A. M.; Park, H. *Nano Lett*. **2006**, *6*, 735.
(31) Gilbert, B.; Huang, F.; Zhang, H.; Waychunas, G. A.; Banfield, J. F. *Science* **2004**, *305*, 651.
(32) (a) Petkov, V.; Gateshki, M.; Niederberger, M.; Ren, Y. *Chem. Mater*. **2006**, *18*, 814. (b) Petkov, V.; Buscaglia, V.; Buscaglia, M. T.; Zhao, Z.; Ren, Y. *Phys. Rev. B*. **2008**, *78*, 054107.
(33) Alpay, S. P.; Misirlioglu, I. B.; Nagarajan, V.; Ramesh, R. *Appl. Phys. Lett*. **2004**, *85*, 2044.
(34) Chu, M. W.; Szafraniak, I.; Scholz, R.; Harnagea, C.; Hesse, D.; Alexe, M.; Gosele, U. *Nat. Mater*. **2004**, *3*, 87.
(35) Catalan, G.; Schilling, A.; Scott, J. F.; Gregg, J. M. *J. Phys.: Condens. Matter* **2007**, *19*, 132201.

1 order of magnitude higher than the coercive field of 7 kV/cm estimated in ref [8b] for switching domains parallel to the field, perpendicular to the substrate. Such a high coercive field in our experiments can be explained by the fact that the field is perpendicular to the switched domains. It is also remarkable the fact that even under an effective electric field of 200 kV/cm, the spontaneous polarization could not be rotated parallel to the field, further confirming that the ferroelectric domain structure is well-stabilized by both electrostatic and elastic energies.

5. Summary and Conclusions

Barium titanate nanowires were obtained by solid-state reaction at 700 °C using titania fiber-like crystals coated with $BaCO_3$ nanoparticles. The morphology of the titania precursor is retained during the reaction with formation of single-crystal $BaTiO_3$ nanowires. Based on the SEM and TEM results, we propose that formation of barium titanate occurs by a topochemical reaction. Therefore, the titania nanowires not only serve as reactant, but can be considered as reactive templates. According to high-energy X-ray diffraction data, the $BaTiO_3$ nanowires have a tetragonal crystal structure with c/a = 1.0045. The presence of several defects, including grain boundaries, dislocations and pores, inside the nanowires is the most likely reason for the depressed tetragonality in comparison to coarse grained ceramics and particles. It should be possible to improve the crystallographic quality of the NWs and, consequently, their ferroelectric properties by growing a $BaCO_3$ coating with uniform thickness by means of chemical vapor deposition or atomic layer deposition. This should guarantee uniform nucleation and reaction conditions over the entire surface of the titania crystals. The ferroelectric properties of individual nanowires were investigated by piezoresponse force microscopy. The PFM measurements show a strong piezoactivity and stripe domain patterns with a domain width of 20−50 nm, predominant in-plane response, and 90° domain walls.

Our results provide evidence of the possibility of fabricating ferroelectric and nonferroelectric 1D nanostructures by solid-state reaction using titania nanowires as reactive templates. The proposed method can be adapted to the synthesis of $SrTiO_3$, $PbTiO_3$, and $Bi_3Ti_4O_{12}$ and might be probably extended to the preparation of other compounds, such as $PbZrO_3$, $Pb(Ti,Zr)O_3$, $LiNbO_3$, $KTaO_3$, etc. Moreover, the use of reactive templates is not limited to 1D nanostructures but allows a rational design of a variety of nanoscale objects by appropriate selection of the template materials, reactions conditions, and geometry.

Acknowledgment. We thank Dr. R. Vormberg, Evonik Degussa GmbH, Germany for having provided us with the titania powder and Dr. Rocco Alessio, Solvay Bario e Derivati, Italy, for having provided us with the barium carbonate powder.